

Large Transverse Thermopower in Shape-Engineered Tilted Leg Thermopile

Ki Mun Bang^a, Sang J. Park^a, Hyun Yu^a, Hyungyu Jin^{a,b,*}

^aDepartment of Mechanical Engineering, Pohang University of Science and Technology (POSTECH), Pohang 37673, South Korea

^bInstitute for Convergence Research and Education in Advanced Technology, Yonsei University, Seoul 03722, South Korea

KEYWORDS: thermoelectric generator, anomalous Nernst effect, tilted leg, thermoelectric thermopile, transverse thermoelectric

* Corresponding author.

E-mail address: hgjin@postech.ac.kr (H. Jin).

Abstract

A transverse thermoelectric (TE) device that employs the Nernst effect can generate an electrical potential by applying a temperature gradient perpendicular to the magnetic field. Anomalous Nernst effect (ANE)-based TE materials have been proposed for transverse TE devices due to their advantage of utilizing internal magnetic field of the materials, which offers the benefit of operating without an external magnetic field. To increase the output voltage of transverse TE devices utilizing ANE, materials with higher ANE coefficients, S_{ANE} , are required. Currently, S_{ANE} reaches $\sim 6 \mu\text{V/K}$ at 300 K; however, it is still lower than the Seebeck coefficient of commercial Bi-Te-based TE materials. As proven in conventional TE research, a meticulous design of device structure has the potential to significantly amplify the output voltage for the given material properties. This study proves the same strategy works for transverse TE devices. We demonstrate that a novel device design, where a shape-engineered tilted-leg thermopile structure is employed, significantly enhance the output voltage in the transverse direction. Owing to shape engineering of the leg geometry, an additional temperature gradient develops along the long direction of the leg, which is perpendicular to the direction of the applied temperature gradient, thereby generating an additional Seebeck voltage V_{SE} that adds to the ANE voltage V_{ANE} . We further show that a simple adjustment of electrode position within the device can further increase V_{SE} . The tilted leg device with electrode adjustment demonstrates a 990% enhanced transverse output voltage compared to that of conventional rectangular leg thermopile-structured devices, wherein only the ANE occurs. This combined output voltage from both the Seebeck effect and ANE is equivalent to what could be achieved by employing materials with the S_{ANE} value of $22.8 \mu\text{V/K}$. This value surpasses the S_{ANE} of state-of-the-art ANE materials and devices currently available. The numerical analysis shows the tendencies of the electrical and thermal outputs of the tilted-leg device, which guides a way to further improve the output voltage. Our study paves a way to

develop highly efficient transverse TE devices that can overcome intrinsic materials challenges by utilizing the degree of freedom of device design.

Nomenclature

RL	Rectangular-leg device
RLW-E	Rectangular-leg device with electrode adjustment
TLW-E	Tilted-leg device with electrode adjustment
L_0	Initial length of the tilted leg (m)
ΔL	Cut off length of the tilted leg (m)
P_{Out}	Output power (W) of the thermopile thermoelectric device
Q''	Heat flux (W/m^2)
R_{CO}	Cut off ratio of the tilted leg
S_{SE}	Seebeck coefficient (V/K)
S_{ANE}	Anomalous Nernst coefficient (V/K)
ΔT	Temperature difference (K)
t	Thickness of the tilted leg (m)
V_{Out}	Output voltage (V) of the thermopile thermoelectric device
V_{SE}	Output voltage (V) generated by Seebeck effect
V_{ANE}	Output voltage (V) generated by anomalous Nernst effect

Greek symbol

θ_{ANE}	Anomalous Nernst angle (= $S_{\text{ANE}}/S_{\text{SE}}$)
-----------------------	---

1. Introduction

Thermoelectric (TE) devices convert waste heat into electrical energy by exploiting the Seebeck effect, in which a temperature gradient across a material generates a difference in the electric potential. Conventional TE devices that employ the Seebeck effect are constructed with a longitudinal structure, wherein the heat flow and electrical output are parallel to each other [1,2]. N- and p-type TE materials are connected into a Π -type structure that requires a large number of legs to increase the output voltage [3]. The complex structure of a longitudinal TE device inevitably leads to large contact resistances between the multiple TE legs and electrodes, which significantly degrades the device efficiency [4]. In contrast, TE devices that utilize the anomalous Nernst effect (ANE) are built in a transverse structure, wherein an electrical potential difference is induced along the direction perpendicular to those of a magnetic field and a temperature gradient. A transverse TE device can be simply fabricated using a single-leg structure and less electrical contacts than a longitudinal TE device [5,6]. A transverse TE device can be easily integrated on a larger scale using significantly fewer manufacturing steps, resulting in a substantial production cost reduction and a simpler device design [4].

One of the key characteristics of transverse TE devices using ANE is the freedom of selecting various thicknesses for device design, whereas the Seebeck effect requires a sufficient length of material along the temperature gradient to generate a large ΔT for usable voltage production. As long as a temperature gradient is present, the output voltage is generated perpendicular to both the temperature gradient and magnetic field; therefore, the ANE can produce voltage regardless of the thickness of the material [7–9]. This effect is well suited for use in TE conversion systems made of thin materials, enabling the design of flexible devices that can fit the curved surfaces of a heat source. This advantage makes the transverse TE devices attractive for a wide range of applications, including IoT devices, wearable devices, *etc* [10,11]. Furthermore, the utilization of ANE for power generation in transverse TE devices

holds the potential to achieve remarkably high energy conversion efficiency [4]. In Seebeck-based TE devices, the Peltier current is induced in the same direction as the Fourier heat. Thus the Peltier effect works in a way to reduce the overall temperature difference in the TE legs, which degrades the conversion efficiency. In contrast, transverse TE devices utilize the Ettingshausen effect to generate a heat current that opposes the Fourier heat and supports device generation [12], thereby increasing the conversion efficiency of TE devices.

Currently, practical deployment of ANE-based transverse TE devices has been limited by small output voltages, mostly due to small anomalous Nernst coefficients of the state-of-the-art materials, two orders of magnitude lower than the Seebeck coefficients of commercial TE materials. To overcome the intrinsic material challenge in realizing practical transverse TE devices, structural engineering of the device becomes imperative, as the device structure design has been proven in conventional TE research to be an effective way to improve overall device performances [13–16]. Previously, transverse devices utilizing ANE has been reported in a thermopile or coiled structure [5,17–19]. The increase in the material length of the transverse TE device can lead to an increase in output performances. Despite these efforts, the resulting devices continue to exhibit low output voltages, ranging from microvolts to a few millivolts, and low output powers, ranging from picowatts to nanowatts [17,18], which can be attributed to their poor material properties [20–28]. Another approach is by using an artificially tilted multilayer structure based on the Seebeck effect [29–32]. N- and p-type TE materials are alternately stacked in a tilted multilayer structure and can generate a non-uniform temperature distribution along the stacked multilayer structure. A tilted structure is used to change the output voltage perpendicular to the direction of heat flow to generate a transverse output voltage. However, attaining thickness reduction poses a challenge for multilayer TE devices utilizing the Seebeck effect. Moreover, the integration of multilayers imparts elevated complexity to the device compared to the single-leg structure of the ANE device. From the

perspective of the ANE device, incorporating the tilted structure into the device utilizing ANE can lead to an enhanced output voltage, while preserving its inherent advantages as a transverse TE device. Therefore, the total transverse output voltage could be further improved by combining the ANE voltage with the Seebeck voltage.

In this study, we propose a novel thermopile TE device by adopting tilted-shaped legs to demonstrate the proof-of-concept of such an idea. We demonstrate that simple geometrical modifications on the thermoelectric legs can lead to a significantly enhanced transverse voltage output, by simultaneously utilizing both Seebeck and anomalous Nernst effects under a unidirectionally applied heat flux. Conventional thermopile devices have rectangular legs and generate an output voltage, V_{ANE} , using only an ANE (Fig. 1a). The shape-engineered tilted leg design not only generates a temperature gradient along the direction of applied heat flux, but also induces an additional temperature gradient along the direction perpendicular to that of the applied heat flux. This additional temperature gradient induces a voltage generated by the Seebeck effect V_{SE} which adds to V_{ANE} (Fig. 1b). Electrodes can also be placed at the hot and cold edges of the end faces to generate additional V_{SE} in the transverse direction. By employing such structure engineering, the output voltage can be increased by 990% compared to that of conventional rectangular-leg thermopile devices wherein only ANE occurs. The effective ANE coefficient S_{ANE} calculated from the combined output voltage of the tilted-leg thermopile TE device surpasses that of the state-of-the-art ANE materials and devices [26,33,34]. Moreover, fabricating the tilted leg thermopile consumes less material for the same dimensions compared to the rectangular leg thermopile, thus presenting a cost-efficient solution. We also conducted numerical analysis by changing the material properties and leg dimensions to provide guidelines for the geometric design of the leg, which could facilitate the subsequent implementation of the suggested concept.

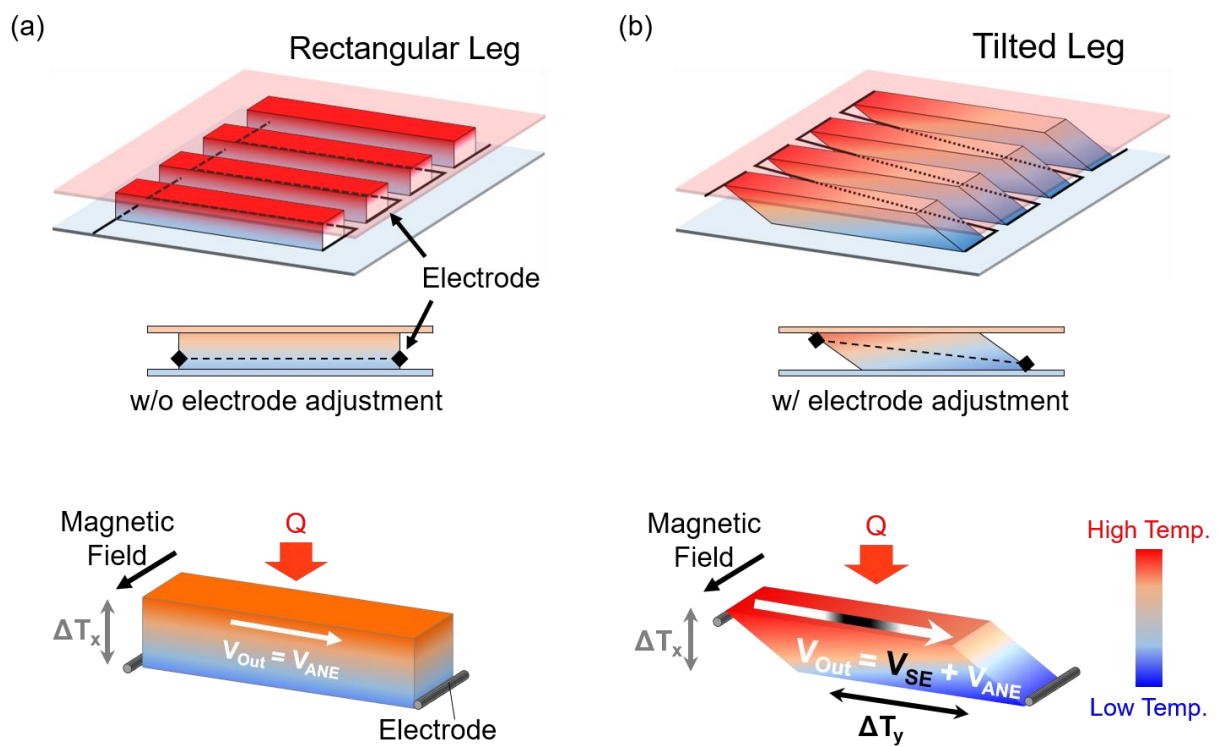


Fig. 1. Schematic illustration of transverse TE devices that use (a) a conventional thermopile with a rectangular leg without electrode adjustment and (b) a shape-engineered tilted leg with electrode adjustment.

2. Experimental Methods

2.1 Fabrication of thermopile device

Fe powder (Alfa Aesar, ~200 mesh, +99.9 %) and Si powder (Sigma–Aldrich, ~325 mesh, 99 %) were mixed at an 3:1 atomic ratio. The powders were formed into cylinders using a press die at 600 MPa for 10 min. The pressed powders were then melted using an arc melter. The melting process was repeated five times to ensure homogeneity. The sample was sealed in a quartz tube under high vacuum ($<10^{-5}$ Torr) and annealed at 1174 K for 24 h and 973 K for 4 h before water quenching. The sample was cut using a diamond wire saw (MTI Korea, STX-202A) into a $1.8 \times 6.66 \times 0.88$ mm rectangular bar. For the tilted-leg device, the sample was cut diagonally to form a right parallelogrammic prism, where the long sides of the prism represent the parallelograms, hence the term “tilted leg”. The tilted leg was fabricated to fit a rectangle size of $1.8 \times 6.66 \times 0.88$ mm (Fig. 2b, 2c), and four legs were used for each device.

To achieve a uniform temperature distribution, a BeO plate (MTI Korea) was cut into 8×10 mm rectangles and utilized as the top and bottom substrates of the heat spreaders. Four legs (both rectangular and tilted) were attached to the bottom substrate using a silver epoxy (Epoxy Technology Inc., EPO-TEK H20E), which was then cured at 400 K for 30 min. Pressure was applied to the top of the legs during curing to uniformly spread the epoxy. The top substrate was then attached to the legs using silver epoxy following the same procedure.

Electrodes were attached to the end faces of the legs. A copper wire (diameter: 0.5 mm) was used as the electrode. The Cu wire was bent into an S-shape, arranged between each pair of legs, attached using silver epoxy, and cured at 400 K for 1 h to complete the fabrication. For the standard rectangular-leg thermoelectric device (RL), the electrodes were attached to the bottom edges of the end faces of the legs (Fig. 2a). For the RL device with electrode adjustment (RLw-E), the electrodes were attached to the bottom of one end face and top of the opposite end face (Fig. 2b). For the tilted-leg device (TLw-E), the electrodes were attached to the acute-

angle edges of the end faces (Fig. 2c). The inclusion of RLW-E was implemented to investigate the influence of the top/bottom placement of the electrodes on the TE effects. This configuration generated an additional Seebeck voltage along the rectangular leg, enabling a comprehensive analysis of the TE performance.

2.2 Material characterization

The electrical and thermal transport properties of the Fe₃Si were measured using a customized nitrogen cryostat system (Cryogenics). Two Cu wires (diameter 0.001 in) were attached to the top and bottom of the bar sample for current inputs, and four Cu wires (diameter 0.001 in) were attached to the two edges of opposite sides of the samples for voltage leads. The standard four-probe method was used to measure the electrical resistance. The Constantan wires of a T-type thermocouple (diameter of 0.001 in) were attached to the two edges of one side to estimate the temperature difference along the sample. A 240 Ω resistive heater was attached to the top of the sample for heating. The Seebeck voltage, Nernst voltage, and temperature difference were measured using a nanovoltmeter (Keithley, 2182A), while the magnetic field was continuously swept between ± 12.5 kOe. All measurements were conducted under a high vacuum environment ($<10^{-6}$ Torr). The stoichiometry was characterized using inductively coupled plasma-optical emission spectroscopy (ICP-OES) analysis (AMETEK, Spectro Arcos). The actual composition of Fe₃Si was similar to the nominal design composition. The measured atomic ratios of Fe and Si were 3.02 and 0.99, respectively, with deviations of 0.02 and 0.01 in the atomic ratio. X-ray diffraction (XRD) analysis confirmed the crystal structure of the material to be a DO3 Fe₃Si structure, without any unexpected structural features (Fig. S1).

2.3 Device characterization

The voltage outputs V_{Out} of the devices were measured using a home-built He cryostat. To measure V_{Out} , each thermopile device was placed on the stage, and a 2000Ω resistance was attached to the device for heating. Thermal grease (Apiezon, H grease) was used to reduce the thermal contact resistance while attaching the device and heater. Currents of 5, 7.07, 8.66, 10, or 11.18 mA were applied to the heater during the measurement, and the experiment was conducted under high vacuum ($<10^{-6}$ Torr) at 300 K. This procedure was repeated for all the devices.

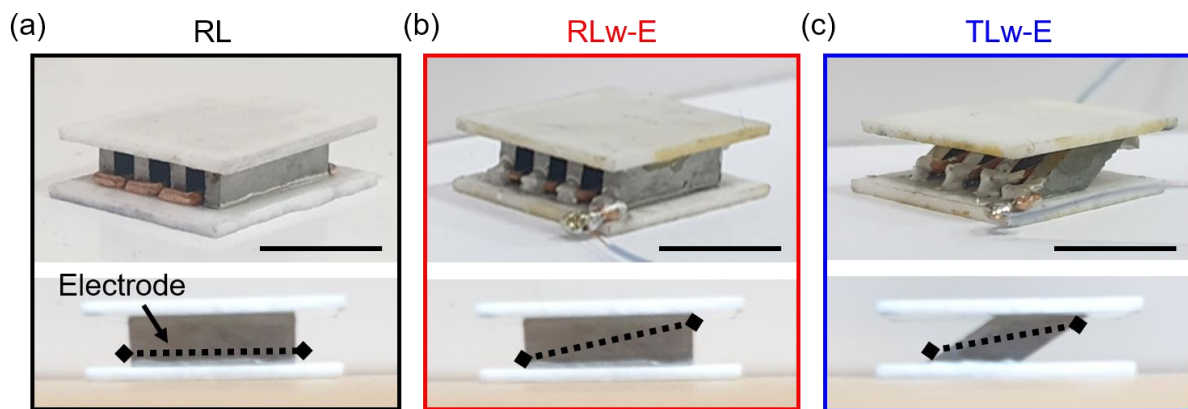


Fig. 2. Photograph of fabricated 4-pair (a) rectangular-leg device (RL), (b) rectangular leg device with electrode adjustment (RLw-E), and (c) shape-engineered tilted leg device with electrode adjustment (TLw-E). Dotted lines: electrode position. Scale bars: 5 mm.

3. Experimental Results and Discussion

The thermal and electrical properties of the synthesized Fe₃Si samples were measured by varying the temperature from 300 to 400 K (Fig. 3). At 300 K, the S_{SE} was $-15.1 \mu\text{V/K}$ and S_{ANE} was $-2.3 \mu\text{V/K}$, and the absolute value of both coefficients increased as the temperature increased (Fig. 3a). The thermal conductivity was $32.9 \text{ W/m}\cdot\text{K}$ at 300 K, which decreased to $31.5 \text{ W/m}\cdot\text{K}$ at 400 K, while the electrical resistivity was $43.1 \mu\Omega\cdot\text{cm}$ at 300 K and increased to $55.6 \mu\Omega\cdot\text{cm}$ at 400 K (Fig. 3b). Fe₃Si was chosen as the tilted-leg device because of its relatively high S_{ANE} near room temperature [28,35]. Additionally, Fe₃Si is composed of earth-abundant elements [36,37], which can reduce the material costs during fabrication compared to other composite materials with a higher S_{ANE} .

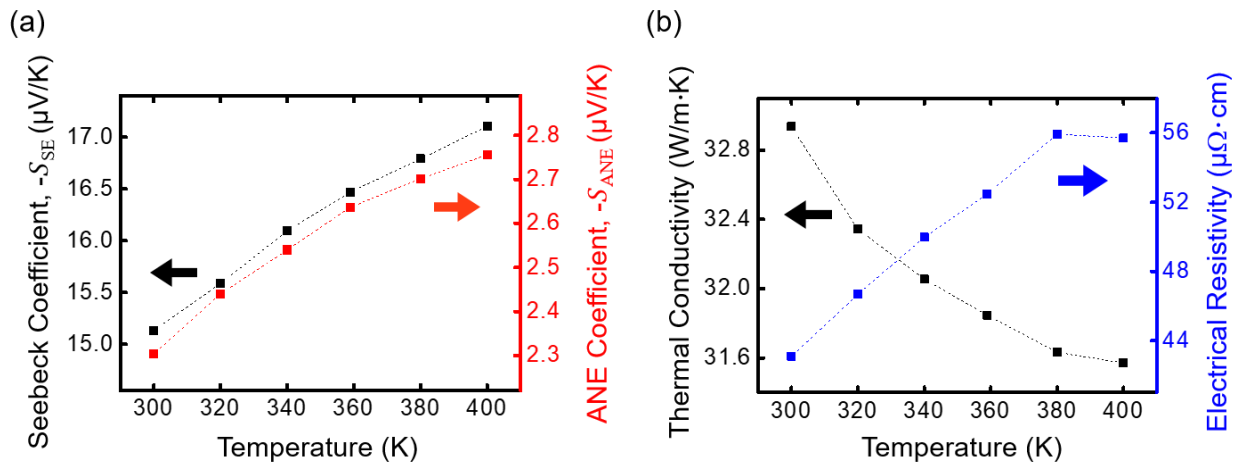


Fig. 3. (a) Seebeck coefficient $-S_{SE}$, anomalous Nernst coefficient $-S_{ANE}$, (b) thermal conductivity, and electrical resistivity of the Fe₃Si sample.

V_{Out} was measured for RL, RLW-E, and TLW-E (Fig. 4). Although both Seebeck and ANE coefficients have negative signs, the output voltages are plotted inversely for simplicity. Each V_{Out} value is the sum of V_{SE} and V_{ANE} . V_{SE} was generated by the shape of the leg, which

shifted the output voltage curve along the Y-axis. V_{ANE} was measured by altering the direction of the magnetic field.

The RL showed $V_{Out} = 0.22 \pm 1.37 \mu\text{V}$, $0.48 \pm 2.86 \mu\text{V}$, $0.84 \pm 4.28 \mu\text{V}$, $1.20 \pm 5.68 \mu\text{V}$, and $1.53 \pm 8.12 \mu\text{V}$ for applied heater powers of 0.03 W, 0.06 W, 0.09 W, 0.12 W, and 0.15 W, respectively (Fig. 4a), and the curves were shifted by 0.22 μV , 0.48 μV , 0.84 μV , 1.20 μV , and 1.53 μV along the Y-axis. In an ideal device, the voltage curve exhibits origin symmetry, indicating that the Seebeck effect does not affect V_{Out} . However, the fabricated RL shows a non-uniform temperature distribution owing to the uneven thermal contact resistance resulting from the fabrication process, leading to the generation of a small V_{SE} in the transverse direction.

The RLw-E showed V_{Out} values of $1.53 \pm 1.89 \mu\text{V}$, $2.66 \pm 3.77 \mu\text{V}$, $3.99 \pm 5.58 \mu\text{V}$, $5.17 \pm 7.53 \mu\text{V}$, and $6.52 \pm 10.48 \mu\text{V}$ for applied heater powers of 0.03 W, 0.06 W, 0.09 W, 0.12 W, and 0.15 W, respectively (Fig. 4b), and the curves were shifted by 1.53 μV , 2.66 μV , 3.99 μV , 5.17 μV , and 6.52 μV along the Y-axis. All these shifts are larger than those in the RL output voltage curves. An additional V_{SE} was generated by changing the location of the electrode diagonally (Fig. 2b).

The TLw-E showed V_{Out} values of $17.0 \pm 1.7 \mu\text{V}$, $34.5 \pm 3.5 \mu\text{V}$, $51.3 \pm 5.4 \mu\text{V}$, $68.8 \pm 7.2 \mu\text{V}$, and $86.2 \pm 9.0 \mu\text{V}$ for applied heater powers of 0.03 W, 0.06 W, 0.09 W, 0.12 W, and 0.15 W, respectively (Fig. 4c), and each voltage curve was shifted by 17.0 μV , 34.5 μV , 51.3 μV , 68.8 μV , and 86.2 μV along the Y-axis. All these shifts were larger than those in both the curves of RL and RLw-E. The tilted geometry induces localized heat flow and increases ΔT in the transverse direction, and adjusting the electrode in the diagonal direction generates a V_{SE} together with the V_{ANE} . Furthermore, the Seebeck coefficient of Cu is one order of magnitude smaller than that of Fe_3Si [38], which generates a smaller voltage when using ΔT . The Seebeck

coefficient of Cu is opposite to that of Fe₃Si, and it additionally increases V_{Out} by diagonally placing the electrode for RLw-E and TLw-E.

The maximum, average, and minimum V_{Out} values of each device increased linearly as the heater power increased. The device performance was determined based on its maximum V_{Out} . A conventional thermopile device with a rectangular leg only generates V_{ANE} in the transverse direction; therefore, the device performance depends only on the amplitude of the V_{ANE} and cannot be increased by changing the direction of the magnetic field. In contrast, the tilted-leg structure distributes heat nonuniformly along the legs to generate V_{SE} , and the saturated voltage is changed by the magnetic field. Therefore, the output voltage can be further increased by selecting an appropriate magnetic field direction.

Compared with the output voltage of RL, the maximum V_{Out} for RLw-E and TLw-E increased to 180% and 990%, respectively (Fig. 4e). This result indicates that using the tilted geometry of the leg can significantly increase the V_{Out} of the device. Using the S_{ANE} of Fe₃Si at 300 K, the effective ANE coefficient S_{ANE} calculated from the combined output voltage is equivalent to that of a device utilizing $|S_{\text{ANE}}|$ of 4.05 $\mu\text{V}/\text{K}$ and 22.8 $\mu\text{V}/\text{K}$ for RLw-E and TLw-E, respectively. The effective ANE coefficient of TLw-E can be achieved through shape engineering of the leg, which is higher than that of state-of-the-art ANE materials at room temperature [27] (Fig. 5). Fe₃Si was selected as the base material in this study because of its earth-abundant composition. The device can further achieve a higher output voltage and equivalent anomalous Nernst thermopower by selecting materials with high S_{ANE} as the base material.

The tilted-leg geometry has the same dimensions as the rectangular leg (Fig. 2) and therefore generates a higher V_{Out} while using less material under the same volume. In addition, RLw-E and TLw-E can operate not only under the magnetic field condition but also in the absence of a magnetic field by exploiting the V_{SE} . This versatility allows the devices to be used

in a wide range of conditions and applications. The measured internal electrical resistance was 9.68Ω for RL, 7.41Ω for RLw-E, and 9.45Ω for TLw-E. At a heater power of 0.15 W , the maximum output power P_{Out} was 7.7 pW for RL, 34 pW for RLw-E, and 0.95 nW for TLw-E. At a heating power of 1.25 W , TLw-E achieved a maximum V_{Out} of $834 \pm 87 \mu\text{V}$ with a maximum P_{Out} of 89 nW (Fig. S2).

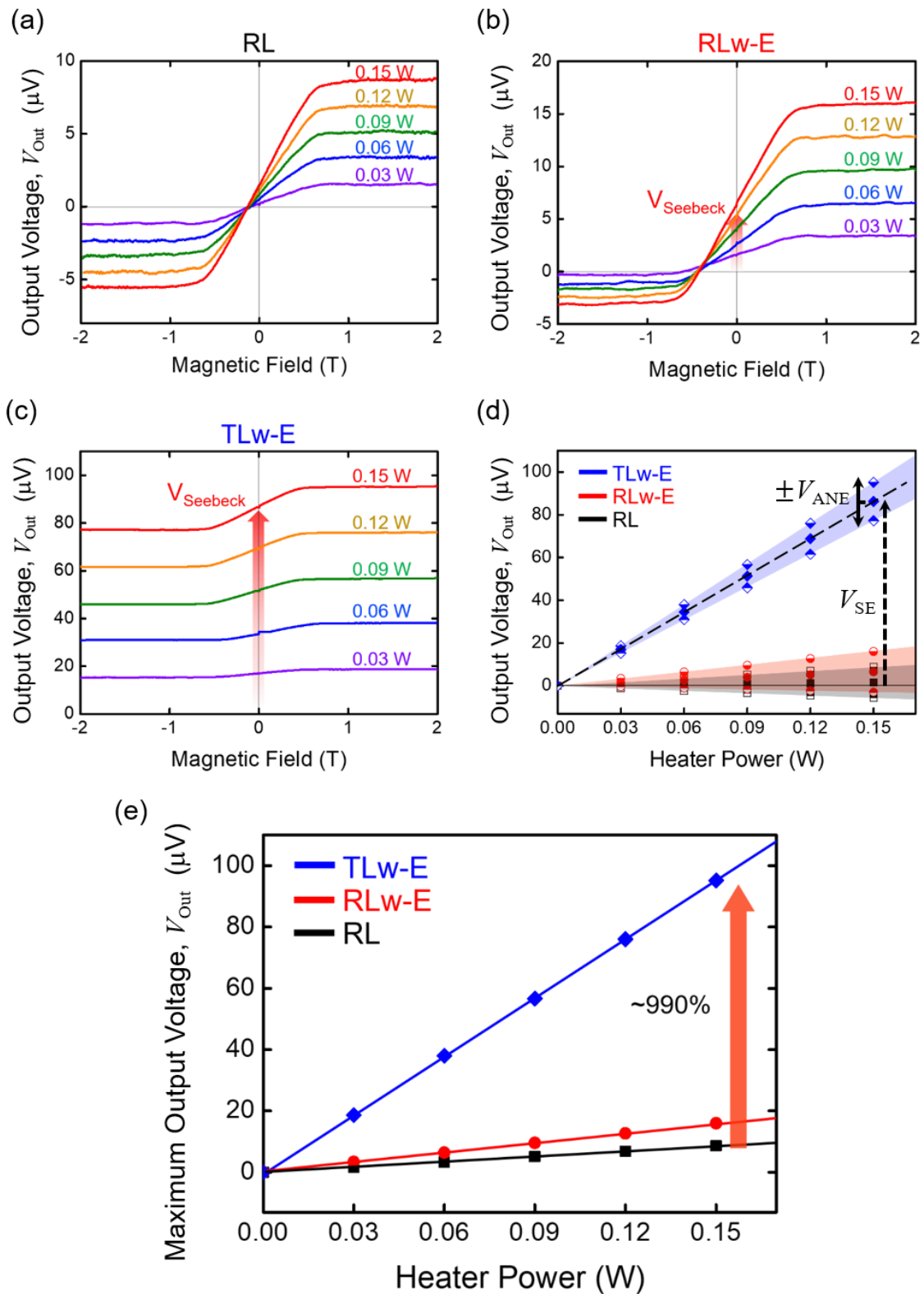


Fig. 4. Output voltages of the (a) rectangular leg device (RL), (b) rectangular leg device with electrode adjustment (RLw-E), (c) and tilted leg device with electrode adjustment (TLw-E) by changing the magnetic field from -2 T to 2 T. The heater power was applied from 0.03 W to 0.15 W. (d) Ranges of the output voltage for each device vs. heater power

(symbol with lower half filled: maximum; filled symbol: midrange; symbol with upper half filled: minimum). (e) Maximum output voltage for each device by changing the heater power. TLw-E shows a 990% increase in the maximum output voltage compared to the RL

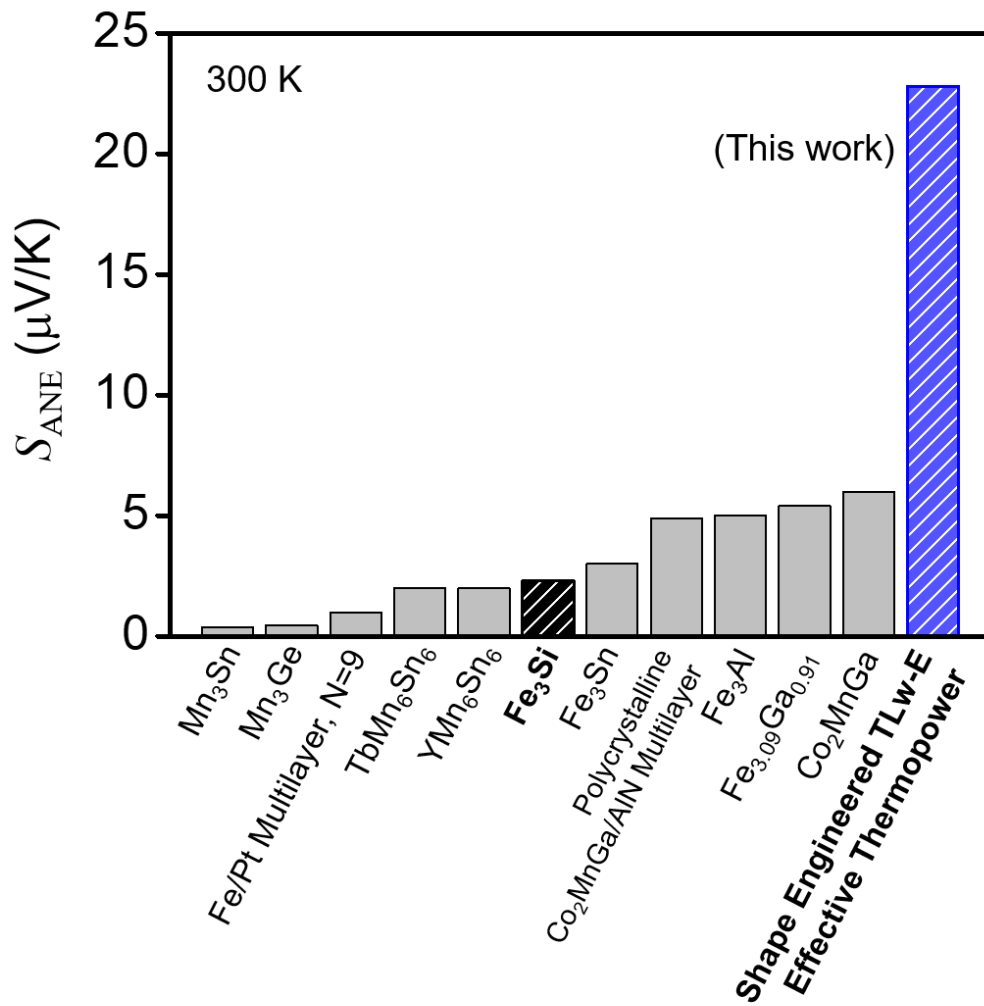


Fig. 5. Anomalous Nernst thermopower of previously reported materials at room temperature. The data include Mn_3Sn [20], Mn_3Ge [39], Fe/Pt multilayer [40], TbMn_6Sn_6 [41], YMn_6Sn_6 [42], Fe_3Si (Rectangular leg), Fe_3Sn [28], polycrystalline $\text{Co}_2\text{MnGa/AlN}$ multilayer [33], Fe_3Al [43], $\text{Fe}_{3.09}\text{Ga}_{0.91}$ [34], Co_2MnGa [26], and effective thermopower calculated from the combined output voltage of the shape engineered tilted leg device with electrode adjustment (TLw-E) studied in this work.

4. Numerical Analysis

Numerical TE analyses were conducted to evaluate the output efficiencies of thermopile devices with tilted-leg structures and conventional rectangular leg structures. The cut off ratio R_{CO} was used to quantify the tilted geometry of the leg, which is defined as the length ΔL of the base of the triangular piece cut off as a proportion of the initial length L_0 of the leg. During the simulation, the Seebeck coefficient matrix was defined such that the diagonal term represented S_{SE} and the off-diagonal term represented S_{ANE} . For simplicity, the absolute values of both S_{SE} and S_{ANE} were used in the matrix. The signs of the coefficients were not considered during the simulation where both S_{SE} and S_{ANE} had negative signs (Fig. 3). The numerical outputs were evaluated by changing R_{CO} , thickness t in the x-direction, and S_{ANE} of the leg (Fig. 6a). The location of the electrode was set for two cases: one with electrodes attached to the entire end face (Fig. 6b) and the other with electrodes attached only to the acute edges of the end faces (Fig. 6c).

Simulations were conducted in four steps. First, V_{Out} of the device and the contributions of V_{SE} and V_{ANE} were monitored by changing the anomalous Nernst angle $\theta_{ANE} = S_{ANE}/S_{SE}$ of the system (Section 4.2). Second, the temperature difference was calculated by varying R_{CO} and L_0 (Section 4.3). Third, V_{Out} , the internal resistance, and P_{Out} were calculated at different locations on the electrode (Section 4.4). Fourth, V_{Out} was calculated for various leg thicknesses (Section 4.5).

4.1 Model geometry and materials

A numerical simulation was conducted for the single-leg device. A rectangular Fe_3Si leg was stacked between the BeO heat spreaders, and a heat flux $Q'' = 100,000 \text{ W/m}^2$ was applied to the top surface of the device, while the bottom temperature was fixed at 300 K (Fig. 6a). The thermal and electrical properties of Fe_3Si were obtained from measured outputs (Fig. 3) and

references [44], and the material properties of BeO were obtained from the COMSOL material library. L_0 was set to 10 mm, and R_{CO} was increased from 0 to 0.5, to form a tilted geometry.

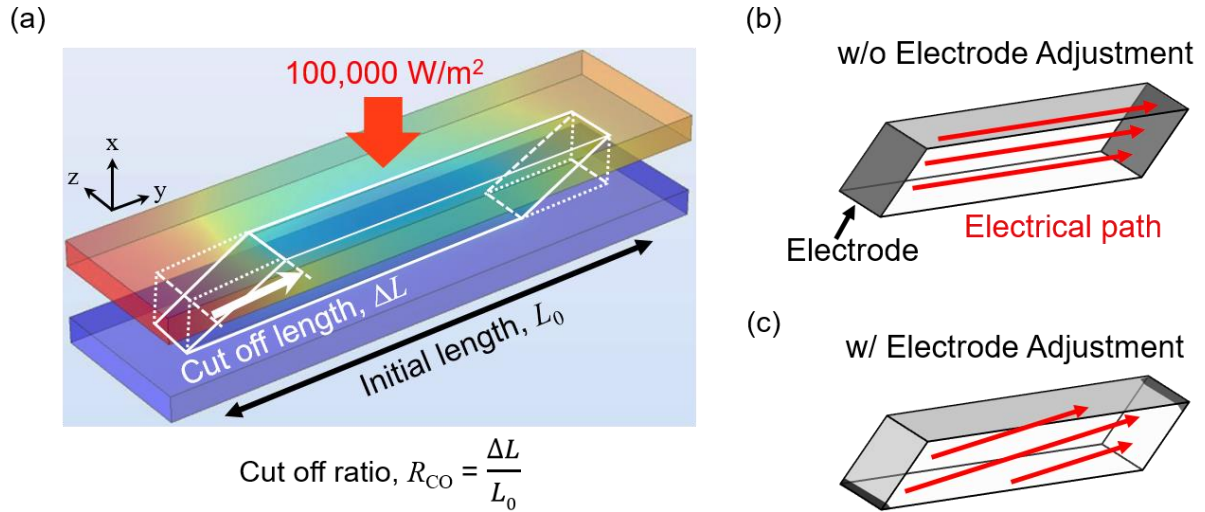


Fig. 6. (a) Boundary conditions for numerical analysis. Schematic illustration of the (b) leg without electrode adjustment and (c) leg with electrode adjustment.

4.2 Evaluation of the output voltage with changes in the cut off ratio and anomalous Nernst angle

First, to simulate the output voltage and the proportion of the voltage contributed by V_{SE} , the anomalous Nernst Angle ($\theta_{ANE} = S_{ANE}/S_{SE}$) was varied (Fig. 7). S_{SE} was fixed at $15 \mu\text{V/K}$, and S_{ANE} was varied from 0 to $150 \mu\text{V/K}$; that is, θ_{ANE} was changed from 0 to 10 [45–47]. For all θ_{ANE} , V_{Out} increased as R_{CO} increased (Fig. 7a). V_{Out} increased more rapidly at a low θ_{ANE} than at a high θ_{ANE} . The proportion of V_{SE} in the total output voltage V_{Out} increased as R_{CO} increased, and its contribution increased rapidly at a low θ_{ANE} (Fig. 7b).

In addition, V_{SE} and V_{ANE} were simulated with various R_{CO} and θ_{ANE} by fixing $L_0 = 10$ mm and $S_{SE} = 15 \mu\text{V/K}$ (Fig. 8). V_{SE} increased as the R_{CO} increased but changed negligibly with an increase in θ_{ANE} (Fig. 8a). The tilted geometry of the leg generates more localized heat

at the pointed edges of the leg than at the obtuse edges, which increases ΔT and leads to the generation of V_{SE} . V_{ANE} changed slightly with variations in R_{CO} , while it increased as the θ_{ANE} increased. Owing to the long leg design, the anomalous Nernst effect became more dominant than the Seebeck effect, resulting in an increased proportion of V_{ANE} in V_{Out} (Fig. 8b).

The utilization of the tilted structure can significantly enhance the output performance of current thermopile TE devices for systems with low θ_{ANE} , despite the current TE materials having a lower S_{ANE} than S_{SE} , which makes the ANE less ideal as a generator. Therefore, a tilted-leg thermopile device can be used as an intermediate system to connect current conventional thermopile TE devices and materials with large values of S_{ANE} .

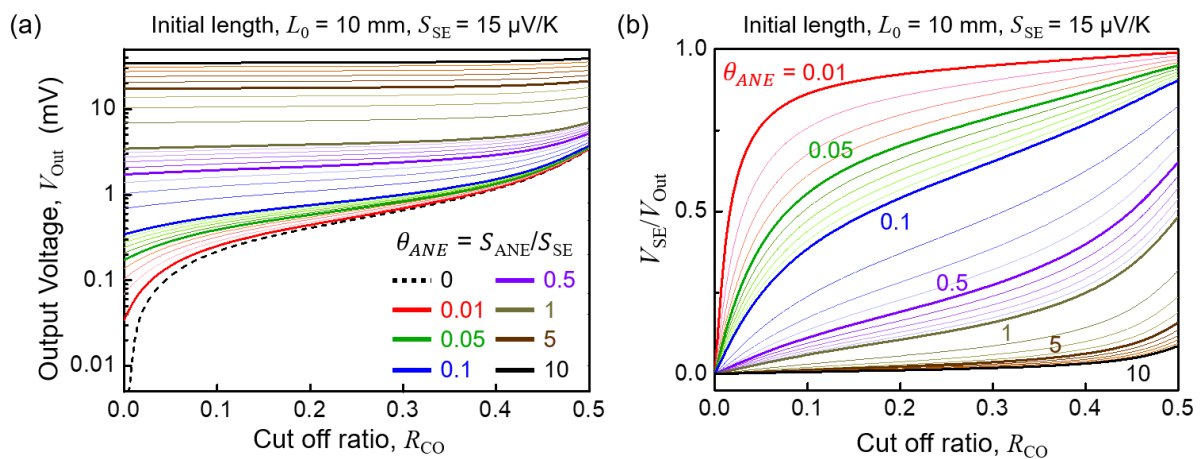


Fig. 7. (a) Output voltage V_{Out} of the tilted-leg device with change in cut-off ratio R_{CO} and anomalous Nernst angle $\theta_{ANE} = S_{ANE}/S_{SE}$. The total length of the device was fixed at 10 mm, and the Seebeck coefficient was fixed at 15 $\mu\text{V}/\text{K}$. (b) V_{SE} as a proportion of total V_{Out} .

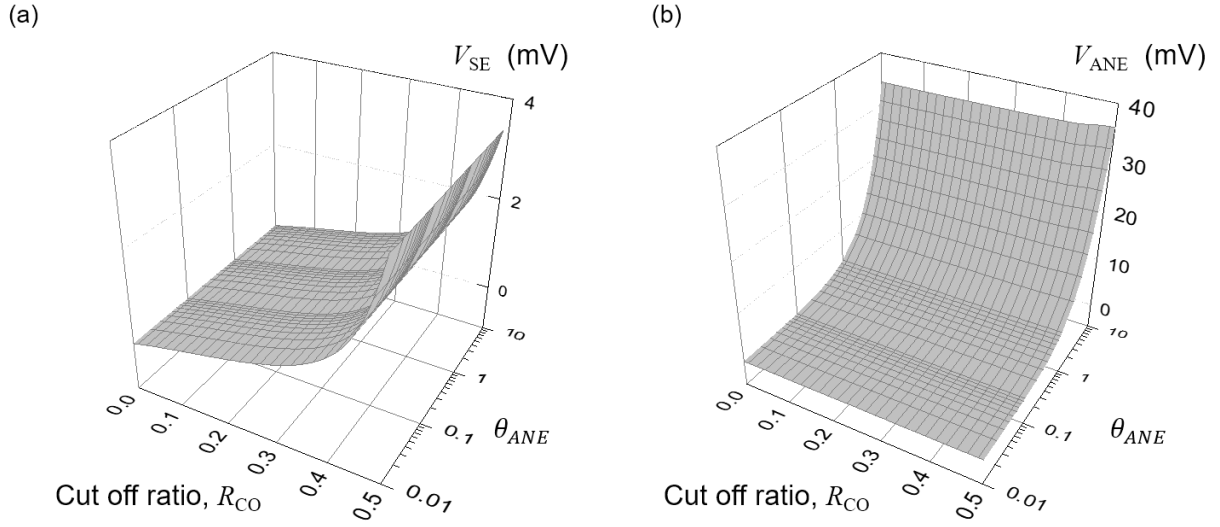


Fig. 8. (a) Output voltage generated by the Seebeck effect V_{SE} (b) and anomalous Nernst effect V_{ANE} of the tilted leg device with a change in the cut-off ratio R_{CO} and anomalous Nernst angle θ_{ANE} ($= S_{ANE}/S_{SE}$). The total length of the device was fixed at 10 mm, and the Seebeck coefficient was fixed at $15 \mu\text{V/K}$.

4.3 Evaluation of the temperature difference with a change in the cut-off ratio and initial length

ΔT between the opposite end faces of the leg (Fig.9a) and between the opposite edges of faces (Fig.9b) were calculated for the cases shown in Fig. 6b and 6c, respectively. Two graphs were plotted by changing the R_{CO} and L_0 of the device. The average ΔT for the side area was 0 K when $R_{CO} = 0$ for all L_0 , where the leg was rectangular; however, as R_{CO} increased, ΔT increased to 200 K at $R_{CO} = 0.5$ (Fig. 9a). The effective area of the thermal heat flow decreased as L_0 decreased, and ΔT increased as L_0 decreased.

The ΔT between diagonally opposite edges of the end faces increased as R_{CO} increased. The device with $L_0 = 6$ mm had the largest ΔT of 43 K at $R_{CO} = 0$, owing to the decrease in the effective heat path area in the vertical direction. For all R_{CO} up to 0.5, ΔT increased as L_0 decreased. At $R_{CO} = 0.5$, ΔT reached 290 K for all devices. For devices with longer L_0 , ΔT

increased rapidly as R_{CO} increased because the tilted-leg geometry became narrower as L_0 increased, leading to an increasingly localized temperature distribution. During the device fabrication, a high ΔT within the leg can degrade the thermal stability of the device. Hence, R_{CO} was limited by the amount of applied heat flux that changed ΔT along the leg.

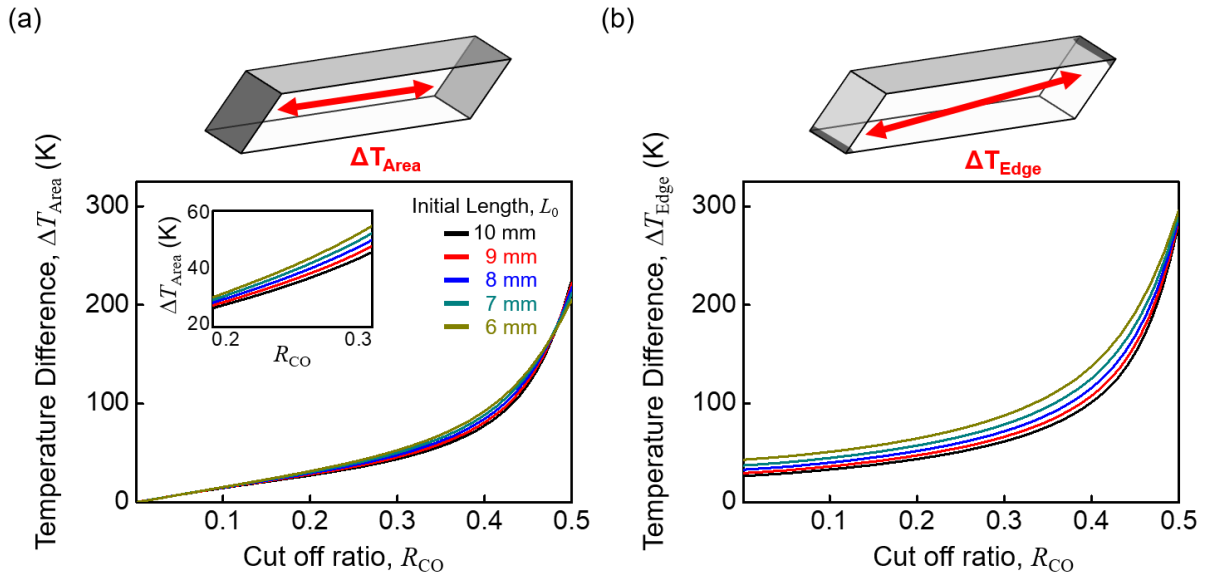


Fig. 9. (a) Average temperature difference ΔT_{Area} between the right and left faces of the leg. Inset: ΔT_{Area} for cut-off ratio $0.2 \leq R_{CO} \leq 0.3$. (b) Temperature difference ΔT_{Edge} between the opposite edges with changing R_{CO} and initial lengths (line colors) of the leg.

4.4 Evaluation of electrical outputs with change of electrode position

The resistance, output voltage, and output power were collected for legs without electrode adjustment (Fig. 10a, 10c, and 10e) and with electrode adjustment (Fig. 10b, 10d, and 10f). The numerical analyses were conducted using various values of L_0 and R_{CO} . The electrodes were located on the end faces of the leg (Fig. 6b) and the electrical field passed along the transverse direction. When the electrodes were located at the acute edges of the opposite-end faces, the electrical field passed diagonally between them (Fig. 6c). First, the electrical resistance decreases for the leg without electrode adjustment (Fig. 10a). Then, as R_{CO} increases and a tilted geometry developed, the effective length of the electrical path decreased with a decrease in the resistance. For the leg with electrode adjustment, the electrical path narrowed near the edges of the end face (Fig. 10b). Increasing the R_{CO} yielded a needle-shaped leg that increased the resistance.

In both electrode configurations, V_{Out} increased as R_{CO} increased (Fig. 10c, 10d). At $R_{CO} = 0.5$, V_{Out} increased to an average of 3.97 mV for the leg without electrode adjustment and to 5.31 mV for the leg with the adjustment. V_{Out} exhibited the same trend as the temperature difference curve (Fig. 9). Therefore, the output power P_{Out} can be calculated for both systems (Fig. 10e, 10f). For the leg without electrode adjustment, an increase in the R_{CO} resulted in the decrease in resistance and an increase in V_{Out} . Consequently, this led to a rapid increase in P_{Out} as R_{CO} increased (Fig. 10e). The leg with electrode adjustment achieved a higher V_{Out} than the leg without electrode adjustment, but the increase in resistance reduced P_{Out} as the R_{CO} increased (Fig. 10f).

In the measured results (Section 3), TLW-E exhibits a higher P_{Out} than RL. During the simulation, the electrodes for the tilted leg were attached directly to the acute edges of the end faces, whereas in the fabricated device, the electrode is a bulk system line that is just attached *near* the edges. Therefore, the increase in internal electrical resistance due to the narrowed path

will be lower than that in the ideal case, and numerical analysis of the leg with electrode adjustment showed a lower P_{Out} than that of the leg without electrode adjustment.

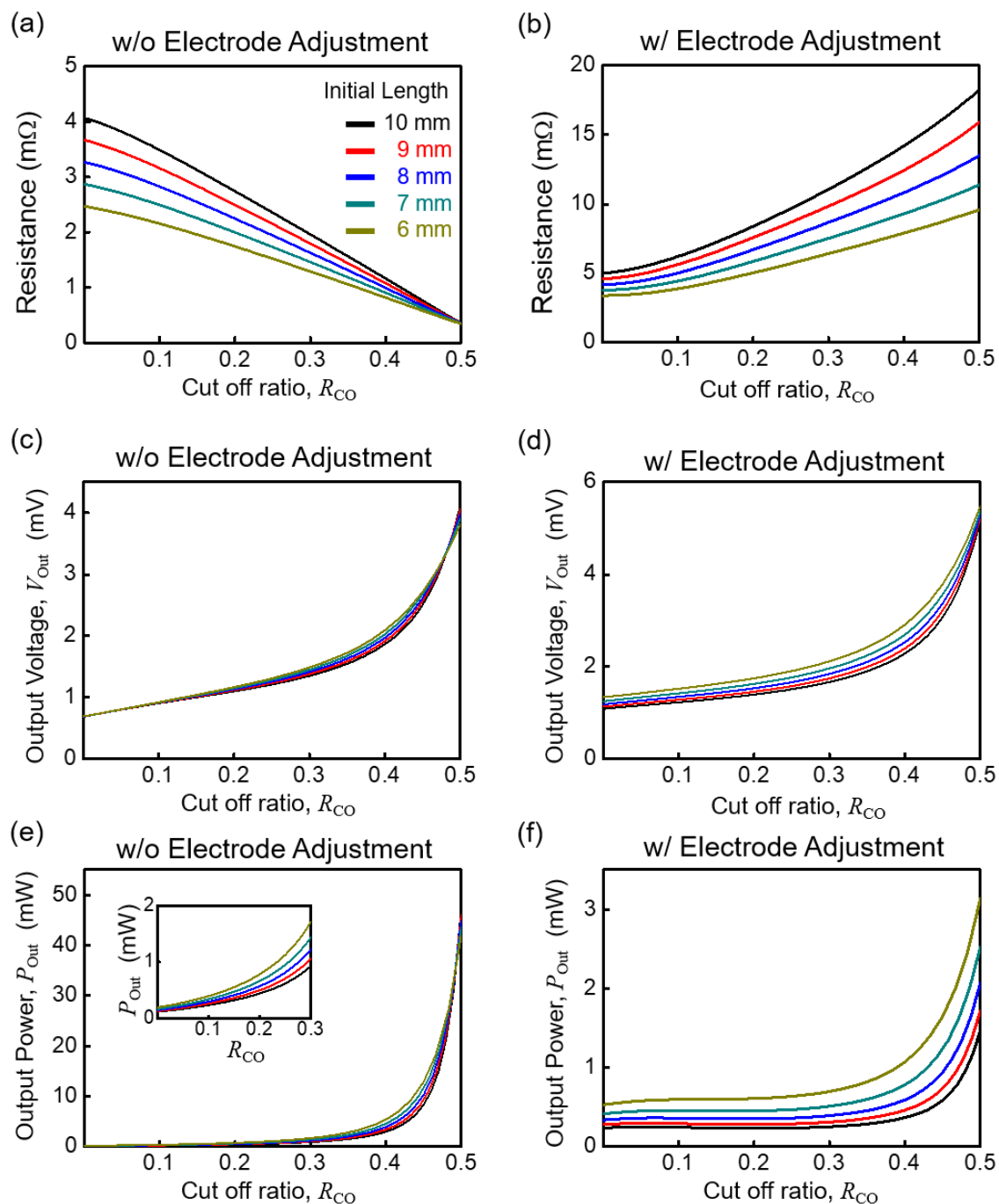


Fig. 10. Numerical analysis for the resistance, output voltage, and output power (a,c,e) of the device without electrode adjustment, and (b,d,f) the device with electrode adjustment. The total length of the device ranged from 6 mm to 10 mm. Inset: output power for cut-off ratio 0 to 0.3.

4.5 Evaluation of output voltage with change of thickness

To investigate the limit of thickness where the ANE device can generate larger V_{Out} than the transverse Seebeck device, the output voltage was compared between the ANE device and the conventional Seebeck-based multilayered structure transverse device [29–32] while decreasing the thickness from 0.1 mm to 0.001 mm. This analysis aimed to assess and evaluate the effectiveness of the ANE device. The numerical analysis was conducted in 2-dimensions for simplicity (Fig. S3a, S3b). As the thickness decreased, the V_{Out} of the Seebeck device decreased because of the insufficient length across the device to generate a large ΔT (Fig. 11). However, the ANE device can generate V_{Out} in the transverse direction using only the temperature gradient, and a decrease in thickness does not affect V_{Out} . The ANE device exhibited a negligible change in V_{Out} (0.083 mV) over the entire thickness. The intersection where the ANE device outperformed the Seebeck device (Fe/Bi₂Te_{2.7}Se_{0.3} multilayer tilted angle = 50°) occurred near 8 μm . For the ANE device with a thickness from 0.1 mm to 0.001 mm, the V_{Out} increased as the R_{CO} increased (Fig. S3c). Therefore, an increase in R_{CO} can shift the intersection to a higher thickness, where the ANE device outperforms the Seebeck-based transverse device (Fig. 11).

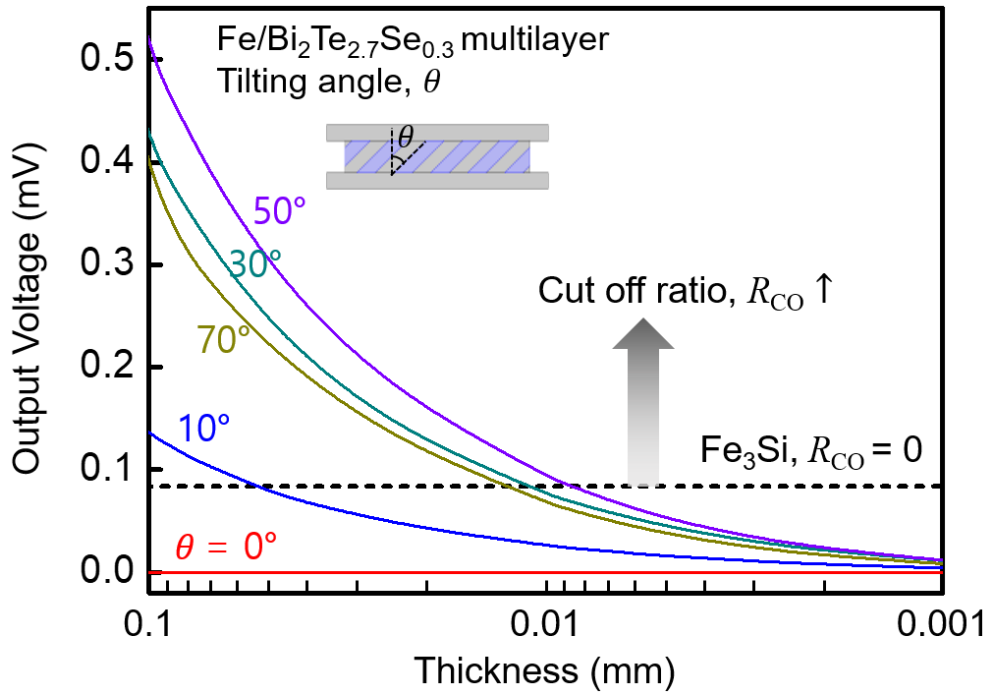


Fig. 11. Output voltage of the ANE device and the Seebeck-based multilayer tilted device for transverse generation [31]. The thickness changed from 0.1 mm to 0.001 mm and the cut-off ratio changed from 0 to 0.5. Fixed values were initial length of device, 10 mm; Seebeck coefficient, $15 \mu\text{V/K}$, and ANE coefficient $3 \mu\text{V/K}$.

5. Conclusions

This study presents a shape-engineered tilted-leg thermopile TE generator to increase the output voltage. Compared with a conventional thermopile device with rectangular legs, the geometry of the tilted structure can artificially generate a localized ΔT along the leg. The shape-engineered tilted leg design not only generates a temperature gradient along the direction of applied heat flux, but also induces an additional temperature gradient along the direction perpendicular to that of the applied heat flux. This additional temperature gradient induces a voltage generated by the Seebeck effect V_{SE} which adds to V_{ANE} in the transverse direction. Additionally, electrodes can be placed at the hottest and coldest edges to generate an additional V_{SE} . Compared with the RL, the RL_{W-E} had a 180% higher V_{Out} , and the TL_{W-E} had a 990% higher V_{Out} , and the effective ANE coefficient S_{ANE} calculated from the combined output voltage is equivalent to that of a device utilizing $|S_{ANE}|$ of 4.05 $\mu\text{V/K}$ and 22.8 $\mu\text{V/K}$, respectively. The results demonstrate that the use of a tilted geometry of the leg and electrode adjustment can significantly improve the performance of thermopile devices. By generating V_{SE} that is independent of the external magnetic field, the thermopile device can be even used in the absence of a magnetic field. This is in contrast to conventional Nernst-based thermopile devices that typically rely on a magnetic field for their functionality. Moreover, the tilted leg thermopile consumes less material for the same dimension compared to the rectangular leg thermopile, thus offering a cost-efficient solution.

Furthermore, a numerical analysis was conducted to provide geometric guidelines for the leg by changing its material properties and dimensions. A material with a small anomalous Nernst angle θ_{ANE} can significantly increase V_{Out} by additionally using V_{SE} . Currently, the TE material used in ANE devices exhibits a smaller S_{ANE} than conventional devices that utilize Bi-Te. The use of a tilted structure can significantly improve the output performance of a thermopile TE device for systems with small θ_{ANE} . Therefore, a tilted-leg thermopile device

can be used as an intermediate system to connect current conventional ANE devices and materials with large values of S_{ANE} . Such systems can provide a way to develop highly efficient transverse TE devices for effective energy harvesting across a wide range of applications, including thin and flexible devices.

CRedit authorship contribution statement

Ki Mun Bang: Conceptualization, Methodology, Validation, Formal analysis, Investigation, Writing - Original Draft, Writing - Review & Editing. **Sang J. Park:** Formal analysis, Investigation, Writing - Review & Editing. **Hyun Yu:** Formal analysis, Investigation, Writing - Review & Editing. **Hyungyu Jin:** Conceptualization, Methodology, Investigation, Resources, Writing - Review & Editing, Supervision, Project administration, Funding acquisition.

Declaration of Competing Interest

The authors declare no competing financial interest.

Acknowledgments:

This work was partly supported by National Research Foundation of Korea (NRF) grant funded by the Korea government (MSIT) (NRF-2020R1C1C1004291, NRF-2022M3C1A3091988) and by National Research Foundation of Korea (NRF) grant funded by the Ministry of Education, Science, and Technology (NRF-2020K1A4A7A02095438) and by Korea Institute of Energy Technology Evaluation and Planning (KETEP) grant funded by the Korea government (MOTIE) (20188550000290, Development of Meta-Silicide Thermoelectric

Semiconductor and Metrology Standardization Technology of Thermoelectric Power module)
and by Basic Science Research Institute Fund (NRF-2021R1A6A1A10042944)

References

- [1] He R, Schierning G, Nielsch K. Thermoelectric Devices: A Review of Devices, Architectures, and Contact Optimization. *Adv Mater Technol* 2018;3. <https://doi.org/10.1002/admt.201700256>.
- [2] Jaziri N, Boughamoura A, Müller J, Mezghani B, Tounsi F, Ismail M. A comprehensive review of Thermoelectric Generators: Technologies and common applications. *Energy Reports* 2020;6:264–87. <https://doi.org/10.1016/j.egy.2019.12.011>.
- [3] Snyder GJ, Toberer ES. Complex thermoelectric materials. *Nature Mater* 2008;7:105–14. <https://doi.org/10.1038/nmat2090>.
- [4] Mizuguchi M, Nakatsuji S. Energy-harvesting materials based on the anomalous Nernst effect. *Sci Technol Adv Mater* 2019;20:262–75. <https://doi.org/10.1080/14686996.2019.1585143>.
- [5] Murata M, Nagase K, Aoyama K, Yamamoto A, Sakuraba Y. Prototype fabrication and performance evaluation of a thermoelectric module operating with the Nernst effect. *IScience* 2021;24. <https://doi.org/10.1016/j.isci.2020.101967>.
- [6] Boona SR, Jin H, Watzman S. Transverse thermal energy conversion using spin and topological structures. *J Appl Phys* 2021. <https://doi.org/10.1063/5.0062559>.
- [7] Mizuguchi M, Ohata S, Hasegawa K, Uchida KI, Saitoh E, Takanashi K. Anomalous nernst effect in an 110-ordered epitaxial FePt thin film. *Appl Phys Express* 2012;5:093002. <https://doi.org/10.1143/APEX.5.093002>.

- [8] Cox CDW, Caruana AJ, Cropper MD, Morrison K. Anomalous Nernst effect in Co₂MnSi thin films. *J Phys D Appl Phys* 2020. <https://doi.org/10.1088/1361-6463/ab4eeb>.
- [9] Seki T, Iguchi R, Takanashi K, Uchida K. Relationship between anomalous Ettingshausen effect and anomalous Nernst effect in an FePt thin film. *J Phys D Appl Phys* 2018. <https://doi.org/10.1088/1361-6463/aac481>.
- [10] Isotta E, Andrade-Arvizu J, Syafiq U, Jiménez-Arguijo A, Navarro-Güell A, Guc M, Saucedo E, Scardi P. Towards Low Cost and Sustainable Thin Film Thermoelectric Devices Based on Quaternary Chalcogenides. *Adv Funct Mater* 2022;32. <https://doi.org/10.1002/adfm.202202157>.
- [11] Lopez-Polin G, Aramberri H, Marques-Marchan J, Weintrub BI, Bolotin KI, Cerdá JI, Asenjo A. High-Power-Density Energy-Harvesting Devices Based on the Anomalous Nernst Effect of Co/Pt Magnetic Multilayers. *ACS Appl Energy Mater* 2022;5:11835–43. <https://doi.org/10.1021/acsaem.2c02422>.
- [12] Nolas GS, Sharp J, Goldsmid J. *Thermoelectrics: basic principles and new materials developments*. 2013.
- [13] He R, Schierning G, Nielsch K. Thermoelectric Devices: A Review of Devices, Architectures, and Contact Optimization. *Adv Mater Technol* 2018;3. <https://doi.org/10.1002/admt.201700256>.
- [14] Shittu S, Li G, Zhao X, Ma X. Review of thermoelectric geometry and structure optimization for performance enhancement. *Appl Energy* 2020;268:115075. <https://doi.org/10.1016/j.apenergy.2020.115075>.

- [15] Cao T, Shi XL, Chen ZG. Advances in the design and assembly of flexible thermoelectric device. *Prog Mater Sci* 2023;131:101003.
<https://doi.org/10.1016/j.pmatsci.2022.101003>.
- [16] Zhang Q, Deng K, Wilkens L, Reith H, Nielsch K. Micro-thermoelectric devices. *Nat Electron* 2022;5:333–47. <https://doi.org/10.1038/s41928-022-00776-0>.
- [17] Sakuraba Y, Hasegawa K, Mizuguchi M, Kubota T, Mizukami S, Miyazaki T, Takanashi K. Anomalous nernst effect in L10-FePt/MnGa thermopiles for new thermoelectric applications. *Appl Phys Express* 2013;6:0–4.
<https://doi.org/10.7567/APEX.6.033003>.
- [18] Yang Z, Codecido EA, Marquez J, Zheng Y, Heremans JP, Myers RC. Scalable Nernst thermoelectric power using a coiled galfenol wire. *AIP Adv* 2017;7.
<https://doi.org/10.1063/1.5003611>.
- [19] Zhou W, Sakuraba Y. Heat flux sensing by anomalous Nernst effect in Fe-Al thin films on a flexible substrate. *Appl Phys Express* 2020;13.
<https://doi.org/10.35848/1882-0786/ab79fe>.
- [20] Ikhlas M, Tomita T, Koretsune T, Suzuki MT, Nishio-Hamane D, Arita R, Otani Y, Nakatsuji S. Large anomalous Nernst effect at room temperature in a chiral antiferromagnet. *Nat Phys* 2017;13:1085–90. <https://doi.org/10.1038/nphys4181>.
- [21] Suryanarayanan R, Gasumyants V, Ageev N. Anomalous Nernst effect in La_{0.88}MnO₃. *Phys Rev B* 1999. <https://doi.org/10.1103/physrevb.59.r9019>.
- [22] Miyasato T, Abe N, Fujii T, Asamitsu A, Onoda S, Onose Y, Nagaosa N, Tokura Y. Crossover behavior of the anomalous hall effect and anomalous nernst effect in

- itinerant ferromagnets. *Phys Rev Lett* 2007.
<https://doi.org/10.1103/PhysRevLett.99.086602>.
- [23] Pu Y, Chiba D, Matsukura F, Ohno H, Shi J. Mott relation for anomalous hall and nernst effects in $\text{Ga}_{1-x}\text{Mn}_x\text{As}$ ferromagnetic semiconductors. *Phys Rev Lett* 2008.
<https://doi.org/10.1103/PhysRevLett.101.117208>.
- [24] Pan Y, Le C, He B, Watzman SJ, Yao M, Gooth J, Heremans JP, Sun Y, Felser C. Giant anomalous Nernst signal in the antiferromagnet YbMnBi_2 . *Nat Mater* 2022;21:203–9. <https://doi.org/10.1038/s41563-021-01149-2>.
- [25] You Y, Lam H, Wan C, Wan C, Zhu W, Han L, Bai H, Zhou Y, Qiao L, Chen T, Pan F. Anomalous Nernst Effect in an Antiperovskite Antiferromagnet. *Phys Rev Appl* 2022;18:1. <https://doi.org/10.1103/PhysRevApplied.18.024007>.
- [26] Guin SN, Manna K, Noky J, Watzman SJ, Fu C, Kumar N, Schnelle W, Shekhar C, Sun Y, Gooth J, Felser C. Anomalous Nernst effect beyond the magnetization scaling relation in the ferromagnetic Heusler compound Co_2MnGa . *NPG Asia Mater* 2019;11. <https://doi.org/10.1038/s41427-019-0116-z>.
- [27] Sakai A, Mizuta YP, Nugroho AA, Sihombing R, Koretsune T, Suzuki MT, Takemori N, Ishii R, Nishio-Hamane D, Arita R, Goswami P. Giant anomalous Nernst effect and quantum-critical scaling in a ferromagnetic semimetal. *Nat Phys* 2018.
<https://doi.org/10.1038/s41567-018-0225-6>.
- [28] Chen T, Minami S, Sakai A, Wang Y, Feng Z, Nomoto T, Hirayama M, Ishii R, Koretsune T, Arita R, Nakatsuji S. Large anomalous Nernst effect and nodal plane in an iron-based kagome ferromagnet. *Sci Adv* 2022.
<https://doi.org/10.1126/sciadv.abk1480>.

- [29] Mu X, Zhou H, Zhao W, He D, Zhu W, Nie X, Sun Z, Zhang Q. High-performance YbAl₃/Bi_{0.5}Sb_{1.5}Te₃ artificially tilted multilayer thermoelectric devices via material genome engineering method. *J Power Sources* 2019;430:193–200.
<https://doi.org/10.1016/j.jpowsour.2019.04.109>.
- [30] Li Y, Wei P, Zhou H, Mu X, Zhu W, Nie X, Sang X, Zhao W. Geometrical Structure Optimization Design of High-Performance Bi₂Te₃-Based Artificially Tilted Multilayer Thermoelectric Devices. *J Electron Mater* 2020.
<https://doi.org/10.1007/s11664-020-08324-2>.
- [31] Zhou H, Liu H, Qian G, Yu H, Gong X, Li X, Zheng J. Geometrical Optimization and Transverse Thermoelectric Performances of Fe/Bi₂Te_{2.7}Se_{0.3} Artificially Tilted Multilayer Thermoelectric Devices. *Micromachines* 2022.
<https://doi.org/10.3390/mi13020233>.
- [32] Meng X, Fujisaka T, Ito KO, Suzuki RO. Thermoelectric analysis for II-type thermoelectric module with tilted elements. *Mater Res Innov* 2014;18:S4116–21.
<https://doi.org/10.1179/1432891714Z.000000000654>.
- [33] Wang J, Lau YC, Zhou W, Seki T, Sakuraba Y, Kubota T, Ito K, Takanashi K. Strain-Induced Large Anomalous Nernst Effect in Polycrystalline Co₂MnGa/AlN Multilayers. *Adv Electron Mater* 2022;8:1–8. <https://doi.org/10.1002/aelm.202101380>.
- [34] Feng Z, Minami S, Akamatsu S, Sakai A, Chen T, Nishio-Hamane D, Nakatsuji S. Giant and Robust Anomalous Nernst Effect in a Polycrystalline Topological Ferromagnet at Room Temperature. *Adv Funct Mater* 2022;32.
<https://doi.org/10.1002/adfm.202206519>.

- [35] Hamada Y, Kurokawa Y, Yamauchi T, Hanamoto H, Yuasa H. Anomalous Nernst effect in Fe-Si alloy films. *Appl Phys Lett* 2021. <https://doi.org/10.1063/5.0062637>.
- [36] Yaroshevsky AA. Abundances of chemical elements in the Earth's crust. *Geochemistry Int* 2006. <https://doi.org/10.1134/S001670290601006X>.
- [37] Turekian KK, Wedepohl KH. Distribution of the elements in some major units of the earth's crust. *Bull Geol Soc Am* 1961. [https://doi.org/10.1130/0016-7606\(1961\)72\[175:DOTEIS\]2.0.CO;2](https://doi.org/10.1130/0016-7606(1961)72[175:DOTEIS]2.0.CO;2).
- [38] Maciá-Barber E. *Thermoelectric materials: Advances and applications*. 2015. <https://doi.org/10.4032/9789814463539>.
- [39] Chen T, Tomita T, Minami S, Fu M, Koretsune T, Kitatani M, Muhammad I, Nishio-Hamane D, Ishii R, Ishii F, Arita R. Anomalous transport due to Weyl fermions in the chiral antiferromagnets $Mn_3 X$, $X = Sn, Ge$. *Nat Commun* 2021;12:1–14. <https://doi.org/10.1038/s41467-020-20838-1>.
- [40] Uchida KI, Kikkawa T, Seki T, Oyake T, Shiomi J, Qiu Z, Takanashi K, Saitoh E. Enhancement of anomalous Nernst effects in metallic multilayers free from proximity-induced magnetism. *Phys Rev B - Condens Matter Mater Phys* 2015;92:1–6. <https://doi.org/10.1103/PhysRevB.92.094414>.
- [41] Xu X, Yin JX, Ma W, Tien HJ, Qiang X Bin, Reddy PVS, Zhou H, Shen J, Lu HZ, Chang TR, Qu Z. Topological charge-entropy scaling in kagome Chern magnet $TbMn_6Sn_6$. *Nat Commun* 2022;13:1–7. <https://doi.org/10.1038/s41467-022-28796-6>.
- [42] Roychowdhury S, Ochs AM, Guin SN, Samanta K, Noky J, Shekhar C, Vergniory MG, Goldberger JE, Felser C. Large Room Temperature Anomalous Transverse

- Thermoelectric Effect in Kagome Antiferromagnet YMn_6Sn_6 . *Adv Mater* 2022;34:1–8. <https://doi.org/10.1002/adma.202201350>.
- [43] Sakai A, Minami S, Koretsune T, Chen T, Higo T, Wang Y, Nomoto T, Hirayama M, Miwa S, Nishio-Hamane D, Ishii F. Iron-based binary ferromagnets for transverse thermoelectric conversion. *Nature* 2020;581:53–7. <https://doi.org/10.1038/s41586-020-2230-z>.
- [44] Miles J, Smith T, Finlayson T. Thermal Expansion of Fe_2MnSi . *Aust J Phys* 1988;41:781. <https://doi.org/10.1071/ph880781>.
- [45] Sheng P, Sakuraba Y, Lau YC, Takahashi S, Mitani S, Hayashi M. The spin Nernst effect in tungsten. *Sci Adv* 2017. <https://doi.org/10.1126/sciadv.1701503>.
- [46] Luo H, Li Q, Du K, Xu Z, Zhu H, Liu D, Cai L, Ghosh P, Qiu M. An ultra-thin colored textile with simultaneous solar and passive heating abilities. *Nano Energy* 2019;65:103998. <https://doi.org/10.1016/j.nanoen.2019.103998>.
- [47] Hu J, Zhang Y, Cabero MAZ, Wei B, Tu S, Liu S, Yu D, Ansermet JP, Granville S, Yu H. Anomalous Nernst effect in Co_2MnGa thin films with perpendicular magnetic anisotropy. *J Magn Magn Mater* 2020;500:3–6. <https://doi.org/10.1016/j.jmmm.2020.166397>.

Large Transverse Thermopower in Shape-Engineered Tilted Leg Thermopile

Supporting Information

Ki Mun Bang^a, Sang J. Park^a, Hyun Yu^a, Hyungyu Jin^{a,b,*}

^a*Department of Mechanical Engineering, Pohang University of Science and Technology (POSTECH), Pohang 37673, South Korea*

^b*Institute for Convergence Research and Education in Advanced Technology, Yonsei University, Seoul 03722, South Korea*

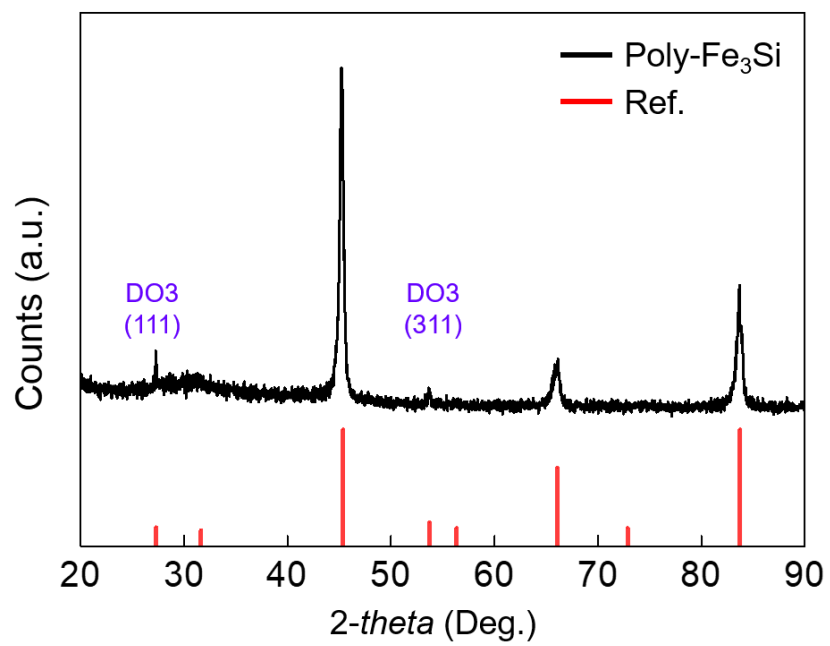


Fig. S1. XRD pattern of the Fe₃Si sample.

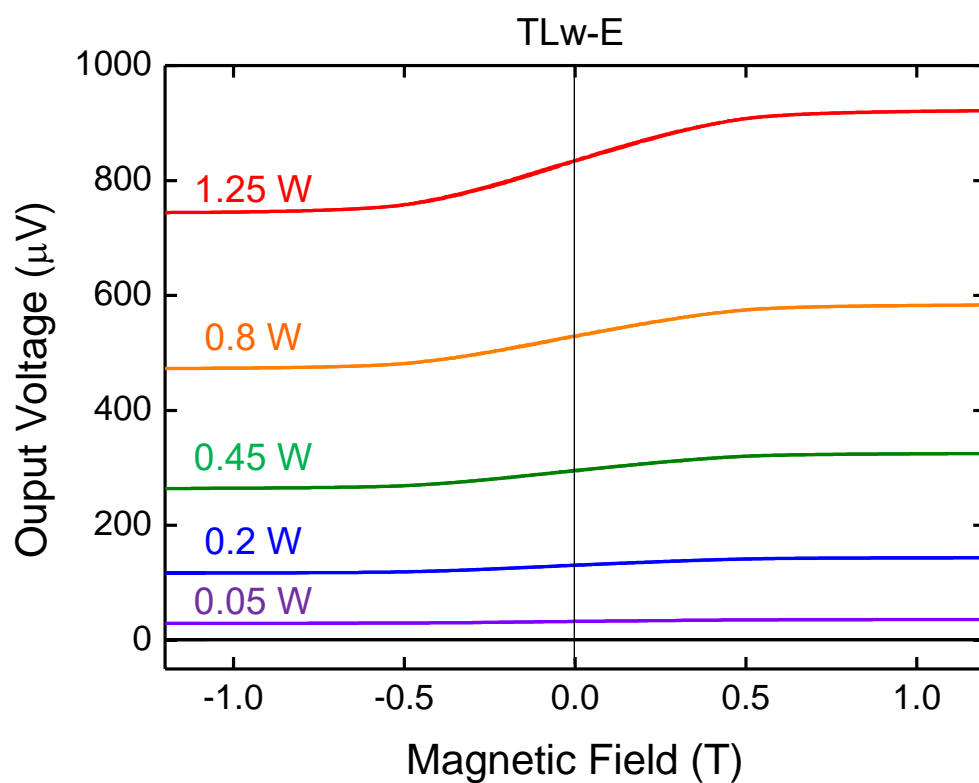


Fig. S2. Output voltages of the tilted leg device with electrode adjustment (TLw-E) by changing the magnetic field from -2 T to 2 T. The heater power was applied from 0.05 W to 1.25 W.

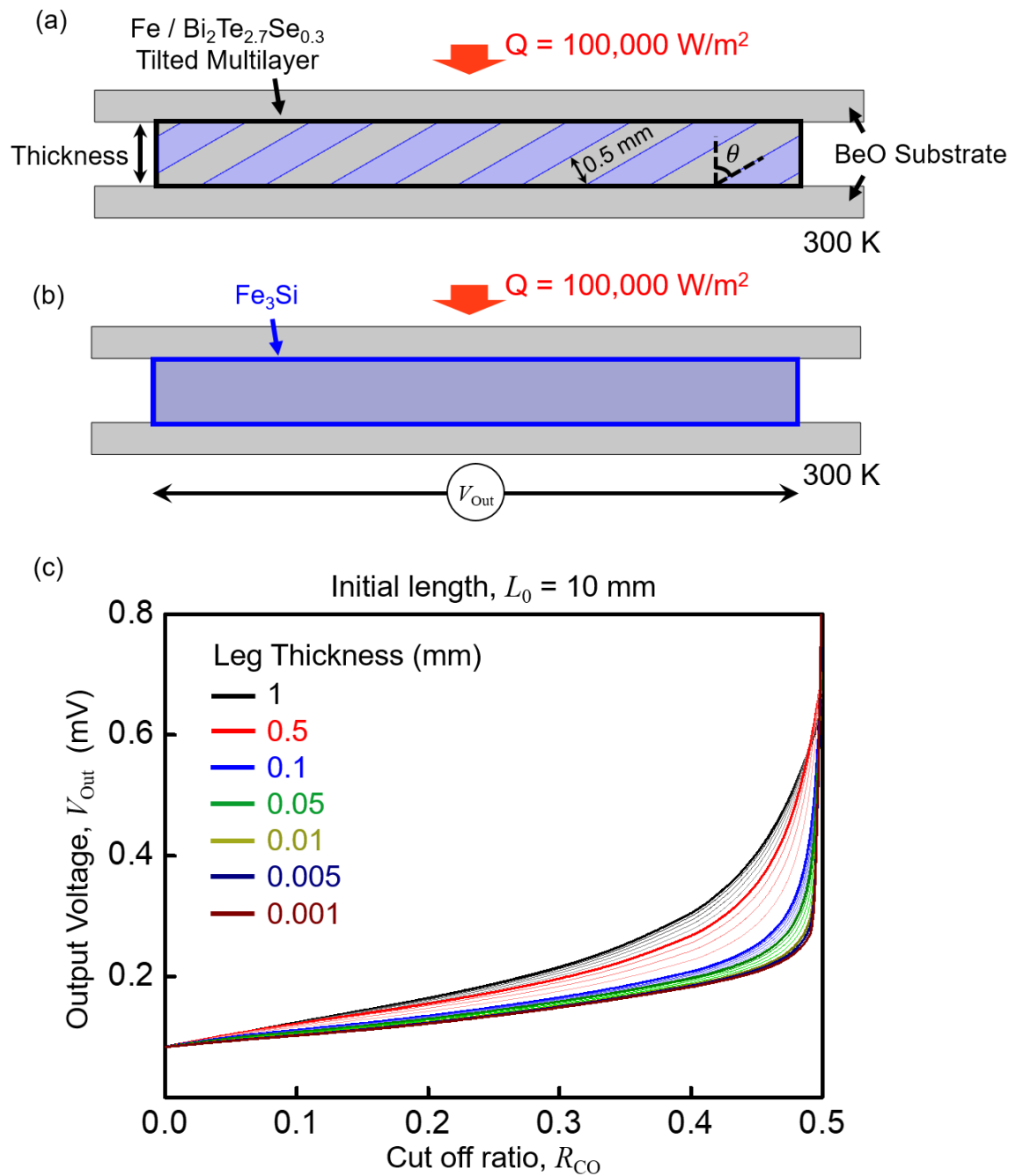


Fig. S3. Boundary conditions of (a) the Seebeck-based multilayer tilted device and (b) the ANE device. (c) Output voltage of the tilted-leg device by changing the thickness from 1 mm to 0.001 mm and cut-off ratio from 0 to 0.5. The fixed values were the initial length of the device, 10 mm; Seebeck coefficient, $15 \mu\text{V/K}$; and ANE coefficient, $3 \mu\text{V/K}$.

The V_{Out} of the device was analyzed by changing its thickness and R_{CO} while keeping L_0 fixed at 10 mm. The V_{Out} increased rapidly with increasing R_{CO} . The ANE device uses a thermal gradient for voltage generation, which is independent of the device thickness, and V_{Out} showed a negligible change as the thickness decreased for $R_{\text{CO}} = 0$.